





Analysis of ozone in the San Joaquin Valley of California

Donald Dabdub^{a,*}, Laurel L. DeHaan^a, John H. Seinfeld^b

^aDepartment of Mechanical & Aerospace Engineering, University of California, Irvine, CA 92697-3975, USA ^bDepartment of Chemical Engineering, California Institute of Technology, Pasadena, CA 91125, USA

Received 8 August 1997; accepted 8 July 1998

Abstract

The dynamics of ozone in the San Joaquin Valley of central California are studied by systematic diagnostic runs of the three-dimensional SARMAP Air Quality Model. Air quality in the San Joaquin Valley is the result of a complex combination of local and transported emissions. Simulations show that relatively brisk winds at points of inflow to the Valley produce a strong dependence of ozone in the Valley on upwind conditions. Furthermore, NO_x influx from boundaries and local emissions has significantly greater impact on ozone production than ROG influx and emissions. © 1999 Elsevier Science Ltd. All rights reserved.

Keywords: Ozone; San Joaquin Valley; Air quality models

1. Introduction

The San Joaquin Valley of California is consistently among those regions where highest ozone levels in the US are experienced (Lagarias and Sylte, 1991; Ranzieri and Thuillier, 1994). High ozone levels in many well studied metropolitan areas, such as the South Coast Air Basin of California, are primarily a result of local emissions. However, in the largely rural San Joaquin Valley it is unclear to what extent episodes of poor air quality are a result of local vs transported emissions.

To investigate air quality in the San Joaquin Valley, the San Joaquin Valley Air Quality Study (SJVAQS) and the Atmospheric Utility Signatures Predictions and Experiments Study (AUSPEX) joined forces in 1989 to form the SJVAQS and AUSPEX Regional Modeling Adaptation Project (SARMAP). This project produced field measurements during 1990 from approximately 160 sites

throughout the Valley, as well as a modeling system consisting of a meteorological model, an emissions inventory model, and an air quality model. The SARMAP Air Quality Model (SAQM) was based on the Regional Acid Deposition Model (RADM) developed by Chang et al. (1987), and has undergone a number of improvements including an updated advection scheme and an updated chemical mechanism. A detailed description of the model is presented by DaMassa et al. (1996).

The goal of this paper is to analyze the nature of ozone formation in the San Joaquin Valley. In particular, this paper address the following questions: How sensitive is ozone in the San Joaquin Valley to initial and boundary conditions, dry deposition, emissions, and winds? To what extent is ozone in the San Joaquin Valley produced from precursors emissions vs boundary conditions? Are the locations in the Valley ROG (reactive organic gases) or NO_x rich? While our principal goal is to diagnose the sources and sinks of ozone in the San Joaquin Valley, we begin the paper with a brief description of the SAQM, including some new features that have been added to the original model. For this study we consider the three day

^{*} Corresponding author. Tel.: (949) 824 6126; fax: (949) 824 8585.

period, 3–5 August 1990, plus a spin-up period, starting on 2 August at noon.

2. Model description

The SARMAP Air Quality Model is designed to compute the concentrations of atmospheric trace species based on the numerical solution of the atmospheric diffusion equation in an Eulerian modeling framework (McRae et al., 1982). Mathematically, the dynamics of each species *i* are described by the following system of conservation equations:

$$\frac{\partial c_i}{\partial t} + \nabla \cdot \mathbf{u} c_i = \nabla \cdot (\mathbf{K} \cdot \nabla c_i) + R_i(\mathbf{c}, T)
+ S_i(\mathbf{x}, t) + \frac{\partial c_i}{\partial t}|_{\text{clouds}},$$
(1)

where $c_i(\mathbf{x}, t)$ are the elements of the gas-phase species concentration vector \mathbf{c} , t is time, $\mathbf{x} = (x, y, z)$, $\mathbf{u} = (u, v, w)$ is the advective flow field, \mathbf{K} is the eddy diffusivity tensor, R_i is the rate of chemical production of species i, T is the temperature, and S_i is the volumetric source of i from emissions and deposition. The last term in Eq. (1) accounts for cloud processes, which are not used in the simulations presented in this paper.

Many components of the model, including vertical diffusion and photolysis rates, are computed according to Chang et al. (1987). The dry deposition parameterization

is based on Chang et al. (1987), but has been modified to account for additional land types that are present in the San Joaquin Valley (Hubbe and Pederson, 1994).

The modeling region of the SAQM is the San Joaquin Valley of California along with the areas surrounding the Valley (Fig. 1). The latitude and longitude of the southwest and northeast corners of the modeling domain are (34.54472, -122.89846) and (39.08257, -118.21475), respectively. The Valley runs from the northwest portion of the model domain to the southeast, and is surrounded by the Coast Range on the southwest and the Sierra Nevada Range on the northeast. The domain is divided into a $12.5 \times 12.5 \text{ km}^2$ regular grid in the horizontal direction. Vertically, the SAQM originally used a 15-layer terrain following σ -coordinate system,

$$\sigma = (p - p_{\text{top}})/p^{\star} \tag{2}$$

$$p^{\star} = p_{\rm s} - p_{\rm top},\tag{3}$$

where p is the pressure at the level where σ is evaluated, p_s is the surface pressure, and p_{top} is the pressure at the top of the modeling region (10 kPa or approximately 16 km). A Surface Layer Submodel (SLS) (Chang et al., 1996) has been added to the original SAQM that has improved the dry deposition and emission resolution of the model. The SLS replaces the bottom layer of the original model with three layers, or two extra levels. Table 1 shows the discretization of the original 16 level vertical grid together with the two additional SLS levels marked "a" and "b". Also in Table 1 are the pressure and

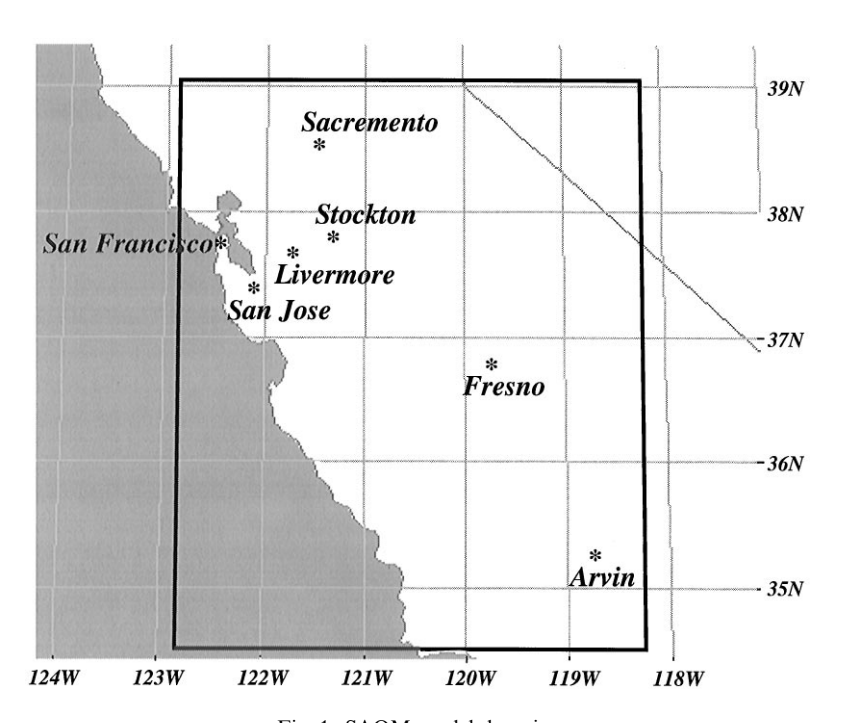


Fig. 1. SAQM model domain.

height corresponding to the sigma levels assuming a 1013 hPa surface and a standard atmosphere. All simulations referred to subsequently include the SLS.

All concentrations and meteorological data are defined at the center of each cell. Eddy diffusivities and the vertical component of the advective flow are defined at the boundaries between layers.

The SAQM uses the Carbon Bond Mechanism, version 4 (CBM4) which consists of 29 differential species (as shown in Table 2) in 83 reactions (Gery et al., 1989).

The temporal approximation of Eq. (1) is obtained from the solution of the operator splitting sequence:

$$\mathbf{c}^{t+2\Delta t} = \mathcal{L}_{x}^{\Delta t} \mathcal{L}_{y}^{\Delta t} \mathcal{L}_{z}^{\Delta t} \mathcal{L}_{z}^{2\Delta t} \mathcal{L}_{c}^{2\Delta t} \mathcal{L}_{z}^{2\Delta t} \mathcal{L}_{z}^{\Delta t} \mathcal{L}_{x}^{\Delta t} \mathcal{L}_{x}^{\Delta t} \mathbf{c}^{t}. \tag{4}$$

The time discretization used in the SAQM is comprised of a basic time step of 5 min for each operator, however each operator has control of its internal time discretization. The time step used by the advection, diffusion, and dry deposition calculations is typically half of the interoperator time step. On the other hand, the time step used in the chemistry operator is significantly smaller and highly dependent on the degree of stiffness of the ordinary differential equations that describe the chemistry. Periods of sunset and sunrise present the highest degree of stiffness, when rapid changes occur in the concentrations of photochemically driven species.

The solution of the advection operator when solving Eq. (1) accounts for the transport of species under a given wind field. The original advection scheme used was the

Table 1 Discretization of the grid using σ -coordinates

Level index	σ-Index	Standard pressure (hPa)	Standard height (m)
15	0.000	100	16170
14	0.156	242	10570
13	0.326	398	7220
12	0.464	524	5220
11	0.600	648	3610
10	0.740	776	2190
9	0.814	843	1520
8	0.866	891	1070
7	0.902	924	770
6	0.918	938	640
5	0.934	953	510
4	0.950	967	390
3	0.966	982	260
2	0.980	995	150
1	0.992	1006	60
b	0.996	1009	30
a	0.9985	1012	10
0	1.000	1013	0

Table 2
Differential species defined in the chemical mechanism

Smolarkiewicz solver (Smolarkiewicz, 1983, 1984). The new advection algorithm incorporated is that described by Bott (1989a, b). Dabdub and Seinfeld (1994) have shown that Bott's solver leads to smaller numerical diffusion and significantly higher accuracy than the Smolarkiewicz algorithm.

2.1. Emissions

Hourly species emissions data are required for each grid cell. Each entry in the emissions inventory database contains the strength of the emission (in g s⁻¹), the emitted species, and the time variation for each source for each grid. The emissions inventory input file processes a raw emissions database using a lumping procedure that is determined by the chemical mechanism. A list of chemical species tracked by the model is given in Table 2. The species accounted for in the emissions inventory are SO₂, SULF, NO₂, NO, ALD, HCHO, PAR, ETH, OLE, ISO, TOL, XYL, CO, and HONO. The emissions inventory used to simulate the August 1990 episode was created using the SARMAP Emission Inventory Model (SEIM), commonly known as GEMAP (Geocoded Emissions Modeling and Projection) (Magliano, 1994). The input data for GEMAP were obtained from the California Air Resources Board.

2.2. Meteorological variables

Three-dimensional wind and temperature fields are provided as hourly input from the SARMAP Meteorological Model (SMM), which is based on the mesoscale meteorological model, MM5 (Grell et al., 1993; Seaman

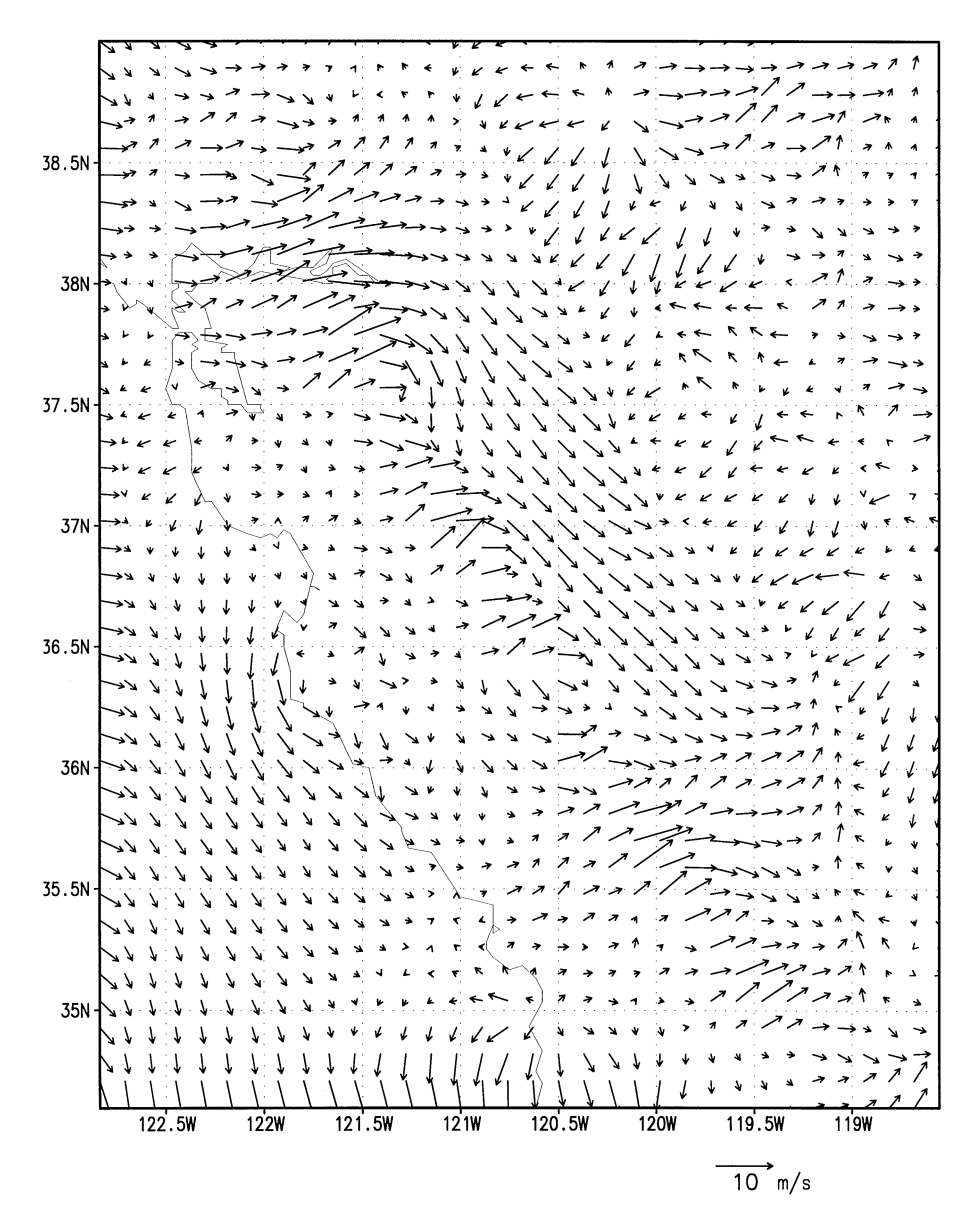


Fig. 2. 1-hour average winds during 1200-1300 h 4 August 1990 at lowest vertical model level.

et al., 1995). A typical daytime, low-level wind flow pattern for the simulation period is shown in Fig. 2. Here, relatively strong winds can be seen coming from the Pacific, through the San Francisco Bay area, and predominantly continuing to the southeast in the Valley. Areas of mountains that surround the Valley generally have weaker, less uniform flow. Nighttime conditions produce stronger downslope flow in the Valley. At sunrise, a cyclonic circulation, known as the Fresno eddy, frequently appears just south of Fresno (Roberts et al., 1995).

2.3. Boundary and initial conditions

The horizontal boundary conditions are

$$u_i c_i - K_{ii} \frac{\partial c_i}{\partial x_i} = F_{b,i}. \tag{5}$$

The horizontal flux, $F_{b,i}$ of species i, at the boundary is computed as

$$F_{\mathbf{b},i} = V_p c_{\mathbf{b},i},\tag{6}$$

where V_p is the normal wind component at the boundary, $c_{\mathbf{b},i}$ is the boundary concentration during inflow conditions, or the concentration next to the boundary during outflow conditions.

The vertical boundary conditions used when solving Eq. (1) are

$$K_{zz} \frac{\partial c_i}{\partial \sigma} = v_{d,i} c_i$$
 at $\sigma = 0.999$, (7)

$$K_{zz} \frac{\partial c_i}{\partial \sigma} = 0$$
 at $\sigma = 0.05$, (8)

where $v_{d,i}$ is the deposition velocity of species *i*. Because of the no-flux condition at the top of the modeling region, predictions are insensitive to upper boundary conditions for species concentration.

Boundary conditions are used to calculate the horizontal flux as described in Eq. (6). Raw data to compute the boundary conditions were obtained from SARMAP field measurements (Blumenthal, 1993). Table 3 shows the low-level boundary mixing ratios that were used for the episode simulated here. The boundary concentrations are assumed to be time independent.

Initial conditions are obtained from available measurements of vertical profiles of the stable species. Short-lived (free radical) species are initialized to zero since the photochemistry will rapidly generate a concentration for each consistent with all other species. Initialization of the simulation is performed by running the model two days prior to the actual simulation period. The resulting concentration field is then used as the initial conditions for the simulation. In Livermore, Fresno, and most sites

Table 3
Boundary mixing ratios for the lowest level of the SAQM used in the 3–5 August, 1990 episode^a

Species code	Mixing ratio (ppb)	Species code	Mixing ratio (ppb)
SO_2	10.0	SULF	0.1
NO_2	2.5	NO	0.5
O_3	40.0	HNO ₃	0.01
H ₂ O ₂	0.01	ALD	1.52
HCHO	5.78	OPEN	0.01
PAR	41.1	ETH	1.4
OLE	0.828	ISO	0.1
NH ₃	10 ⁻⁷	N ₂ O ₅	0.1
NO ₃	0.1	PAN	0.1
TOL CRES	0.1 0.492 0.1 200	XYL MGLY C ₂ O ₃	0.1 0.27 0.1 10^{-7}
HONO CH ₄ HO ₂	0.1 1700 10 ⁻⁷	HNO ₄ HO	0.1 10 ⁻⁷

^aBlumenthal et al. (1993).

in the Valley, essentially identical predictions result from the base case and the zero initial condition case after the spin-up time. The only exceptions are Arvin and other sites in the southeastern portion of the Valley, which become identical to the base case after an additional 24 h.

3. Diagnosis of ozone in the San Joaquin Valley

Diagnostic runs were performed using the SAQM to study the major sources and sinks of ozone in the San Joaquin Valley. In describing our results we will frequently focus on three sites that are representative of the range of those in or adjacent to the Valley: Arvin, Fresno, and Livermore (see Fig. 1). Arvin is a small farming town in the southeast corner of the modeling region; Fresno is a city with a population of approximately 350 000 in the middle of the Valley; Livermore is a suburban city immediately east of the San Francisco Bay area and near the influx boundary of the region. These three sites represent different types of locations and population densities, providing a spectrum of sites that are influenced by material flowing into the Valley as well as by local Valley emissions.

3.1. Base case

There are several key aspects of the dynamics of ozone formation in the San Joaquin Valley that are illustrated by the base case. Over the three-day simulation, highest ozone levels were consistently found in four distinct areas: near the outflow of San Francisco, in the southern portion of the Valley, downwind of Fresno, and in the vicinity of Sacramento. In these locations it was not uncommon for the ozone mixing ratio to exceed 140 ppb during the period. It is observed from the base case simulation that local emissions from San Francisco are transported downwind into the Valley. Throughout the Valley the maximum ozone concentration tends to occur around 4 pm, while the minimum values are more varied, occurring between 4 am and 8 am.

Fig. 3 shows both the observed and the base case predictions of ozone mixing ratio for the three-day period of the simulation at Arvin, Fresno, and Livermore. We note that the average ozone measured in Arvin is greater than that of Fresno or Livermore. This is especially noticeable at night, when ozone in Arvin rarely decreases below 50 ppb. While agreement between the SAQM predictions and observations is quite good, there are discrepancies that will be discussed subsequently. For example, the ozone mixing ratio is predicted to drop earlier in the evening in Fresno than observed, and ozone predictions in Livermore are consistently high during the first two days of the period. However, at Arvin, and at other sites not shown here, agreement between predicted and observed ozone levels is quite close.

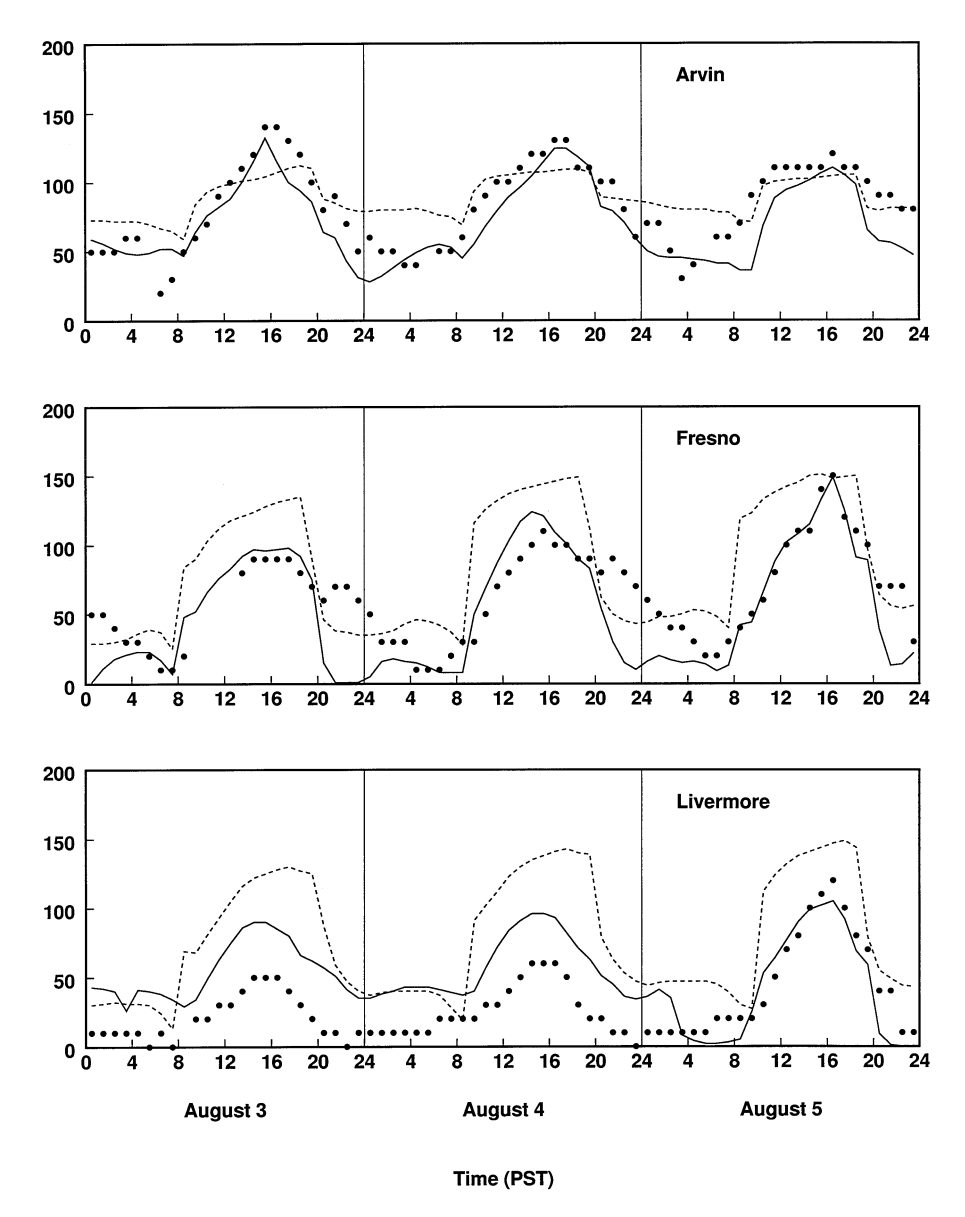


Fig. 3. Ozone mixing ratio (ppb): observations (data points), base case predictions (solid), and predictions with winds set to zero (dashed).

We will now examine the nature of the ozone problem in the San Joaquin Valley using diagnostic runs of the SAQM. In all the following cases, perturbations to the model were implemented from the beginning of the spinup period (noon on 2 August 1990). The figures show ozone mixing ratio beginning 3 August at the lowest vertical level of the model.

3.2. Influence of winds

The topography of the San Joaquin Valley produces an advective flow that varies in direction and magnitude throughout the Valley. The wind in Livermore, which is near the primary inflow into the Valley, is virtually always from the west, and rarely falls below 3 m s⁻¹. The strongest winds in Livermore occur around midnight, at an average speed of over 6 m s⁻¹. Arvin, which is located at the end of the Valley, has a more varied wind field. The strongest winds tend to be in the late evening, and are from the southwest. At other times of the day the wind is from the northwest (early morning), or from the east (late morning). Fresno is slightly east of the main down-Valley flow. In Fresno, a maximum average wind of over 6 m s⁻¹ occurs around 4 am, blowing primarily

eastward. The winds reach a minimum speed in the evening, followed by a few hours of northeastward winds.

In order to understand the effects of the advective flow on ozone formation in the Valley, we have altered the meteorological inputs to SAQM. Fig. 3 shows predicted ozone levels at these sites under completely calm conditions. In Arvin there is a small, but rapid increase in ozone mixing ratio at approximately 8 am, and a small, but rapid decrease around 8 pm. Otherwise, the ozone level remains relatively constant for 12 h. At sunrise the available NO_x catalyzes ozone formation after which the ozone mixing ratio is essentially unchanging. Likewise, in the evening, after the available NO scavenges ozone, there is little variation in the ozone concentration. It can also be seen that in this simulation the daytime ozone values are lower, and the nighttime ozone values are higher than in the base case. This is a result of the relatively small amounts of NO_x present in this rural town. There is little NO₂ to create ozone in the morning, and little NO to remove it in the evening. This suggests that transport of NO_x to Arvin under normal wind conditions is responsible for some of the observed ozone formation.

In the simulation with no wind, both Fresno and Livermore exhibit an increase in ozone mixing ratio from 8 am to 8 pm. The area with the highest increase in ozone mixing ratio in the modeling domain is the San Francisco Bay area (not shown), where peak ozone values tripled in comparison with the base case. Not surprisingly, with no wind this area accumulates local emissions throughout the day and is predicted to exhibit daytime ozone peaks higher than in the base case, implying that emissions from these sites are transported downwind into the Valley under normal wind conditions.

We have also examined the effect of wind on NO_2 concentration (results not shown). As one would expect from observing the ozone behavior, NO_2 increased in Livermore and decreased in Arvin under calm conditions relative to the base case . However, the NO_2 concentration in Fresno also decreased while ozone levels increased. It can be seen from the emissions data that while the San Francisco Bay Area is a primary source of NO_x , the Fresno area is a primary source of many reactive organic gases (ROG). This suggests that the ozone concentration in Fresno is dependent both on ROG, which tend to be locally emitted, and NO_x , which is generally non-local.

Other diagnostic simulations in which wind speeds were reduced by 50 and 75% produced similar results.

3.3. Influence of boundary conditions

Boundary conditions for the base case simulation have been given in Table 3 (Blumenthal, 1993). Air off the California coast, which serves as the boundary conditions in the present study, is contaminated with anthropogenic material from continental sources at levels significantly higher than those found over the mid-Pacific ocean (Winner et al., 1995). As a result, that we will see with the large volume of air being transported

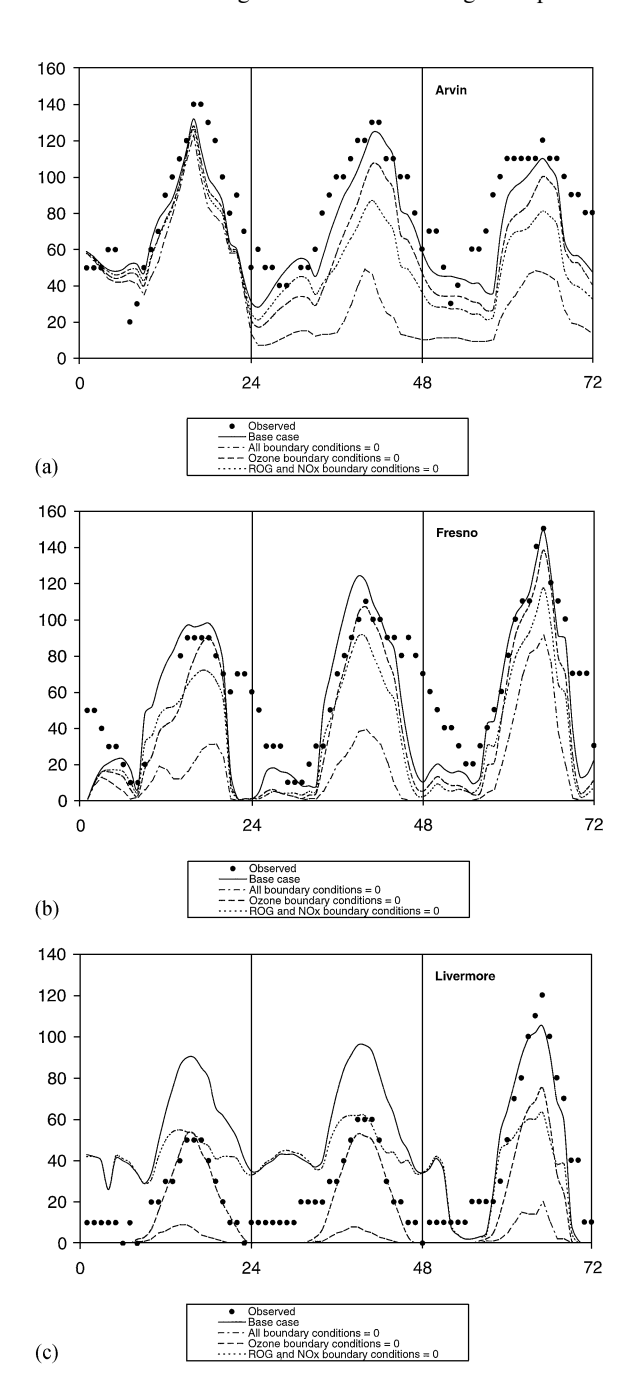


Fig. 4. Ozone mixing ratio (ppb): observations (data points) base case predictions (solid), predictions with all boundary conditions set to zero (dot-dash), predictions with ozone boundary conditions set to zero (large dash), and predictions with ROG and NO_x set to zero (small dash).

into the modeling domain from the ocean, a substantial quantity of ozone and ROG and NO_x precursors flows into the region each day and that this transport exerts a non-trivial effect on air quality over the region.

In order to study the effects of air being transported into the San Joaquin Valley on ozone levels in the Valley, simulations were performed in which the boundary conditions were altered. In the first case the concentrations of ROG, NO_x, and O₃ at the boundaries were set to zero. A zero ozone boundary condition has been used purely diagnostically; a constant 30 ppb background of ozone is present even in cleanest of conditions. Comparison between predictions in the base case and those with zero boundary conditions demonstrates the effect of boundary input on ozone concentrations. One would expect the largest differences to occur in sites near the boundary. Further simulations were made in which a subset of the boundary conditions were set to zero in order to test the sensitivity to specific components.

A large difference between ozone predictions in the base case, and those with all boundary conditions set to zero can be seen in Livermore (Fig. 4), where ozone is predicted to nearly vanish when the boundary conditions are set to zero. This is the response to zero boundary conditions in the entire northwest corner of the region.

Note that this is not a result of extremely low emissions in Livermore, as it was determined previously that Livermore's ozone has a reasonably significant dependence on local emissions. However, there is a larger dependence on boundary conditions because of Livermore's close proximity to the region boundary where there is a large influx of material. In particular, the effect of a constant influx of 40 ppb of ozone from the boundary can generally be seen in Livermore. Fresno also exhibits a notable decrease in ozone levels with zero boundary conditions. However, as expected, this decrease is smaller than that in Livermore, as Fresno is farther from the model boundary than Livermore. Arvin, being the farthest from the influx model boundary, exhibits almost no sensitivity to a change in boundary conditions on the first day of the simulation. It takes approximately 24 h for boundary air to be advected to Arvin.

To test further the sensitivity of ozone predictions to boundary conditions, diagnostic runs were made in which a subset of the boundary species concentrations are altered. When only ozone boundary conditions are set to zero (Fig. 4), both Arvin and Fresno experience small, but noticeable, reductions in ozone concentrations. Livermore, on the other hand, is predicted to experience an ozone loss of approximately 50%. Furthermore, it can be seen that the sole source of nighttime

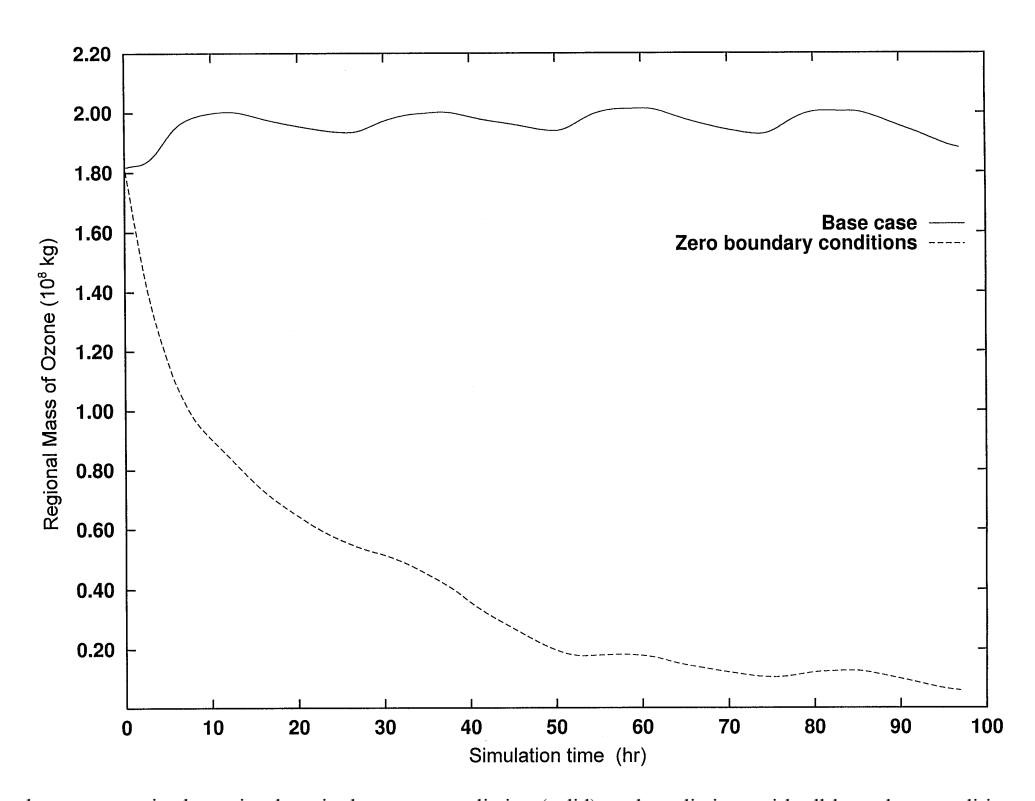


Fig. 5. Total ozone mass in the entire domain: base case prediction (solid), and predictions with all boundary conditions set to zero (dashed).

ozone in Livermore is from advection into the region from the boundary. When only ROG and NO $_x$ boundary conditions are set to zero (Fig. 4), ozone levels in Arvin and Fresno experience somewhat greater reductions than those predicted when only boundary ozone is assumed to be zero. When all boundary conditions are set to zero, ozone levels are reduced by a greater amount than the sum of the reductions produced by ROG + NO $_x$ and O $_3$ separately. Ozone is the major source of odd hydrogen which initiates the process of ozone formation. When ozone is not zero at the boundaries, the relative importance of ROG and NO $_x$ decreases.

An overall evaluation of the effect of boundary conditions on ozone predictions is shown in Fig. 5, which shows the integrated total mass of ozone for the base case and that with zero boundary conditions. The rapid decrease in ozone mass over time when all boundary conditions are set to zero points clearly to the significant effect exerted by the species boundary conditions on predicted ozone in the San Joaquin Valley.

Much of the sensitivity to the boundary conditions can be explained by the meteorology of the area. Because of high winds that blow in from the Pacific, any species advected in from sources over the Pacific have

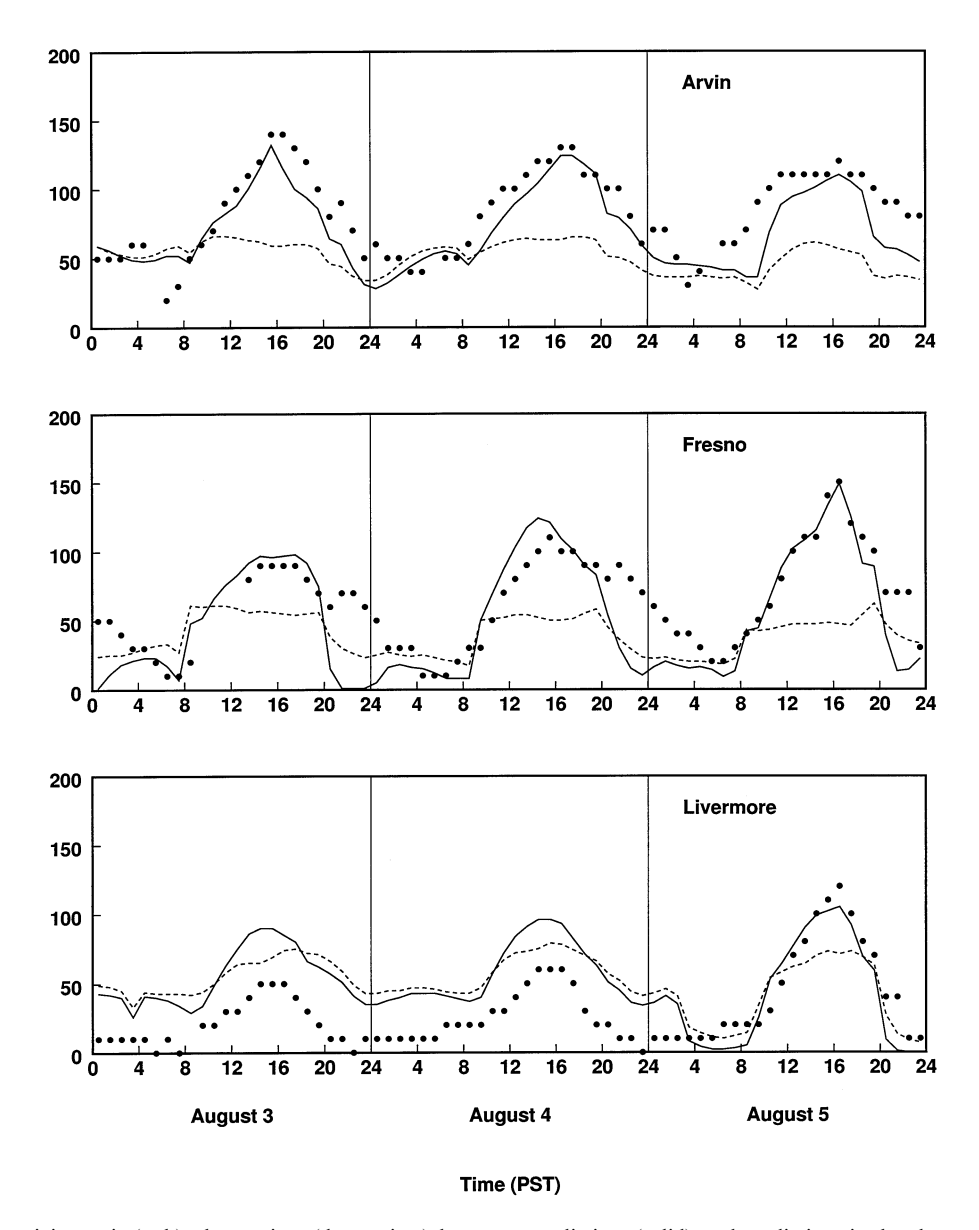


Fig. 6. Ozone mixing ratio (ppb): observations (data points), base case predictions (solid), and predictions in the absence of emissions (dashed).

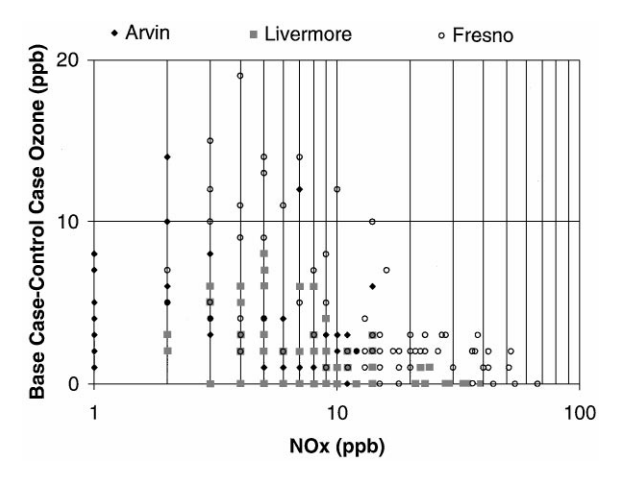


Fig. 7. Response of ozone formation to 50% ROG reductions in emissions vs concurrent NO_x mixing ratios for Arvin (solid diamond), Livermore (solid square) and Fresno (circle). Each data point corresponds to each hourly averaged mixing ratio during 3–5 August 1990.

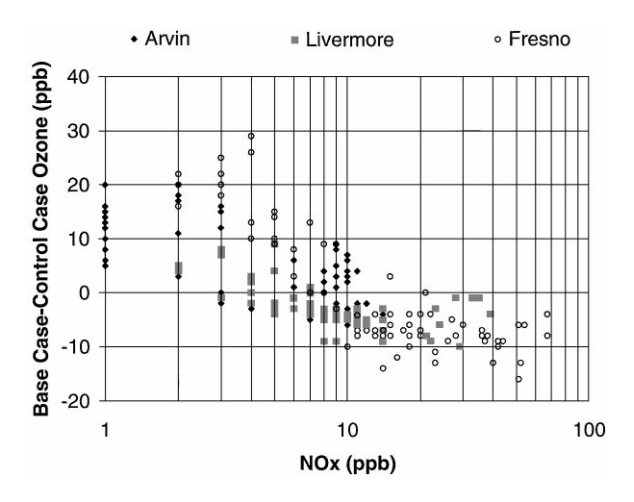


Fig. 8. Response of ozone formation to 50% NO_x reductions in emissions versus concurrent NO_x mixing ratios for Arvin (solid diamond), Livermore (solid square) and Fresno (circle). Each data point corresponds to each hourly averaged mixing ratio during 3–5 August 1990.

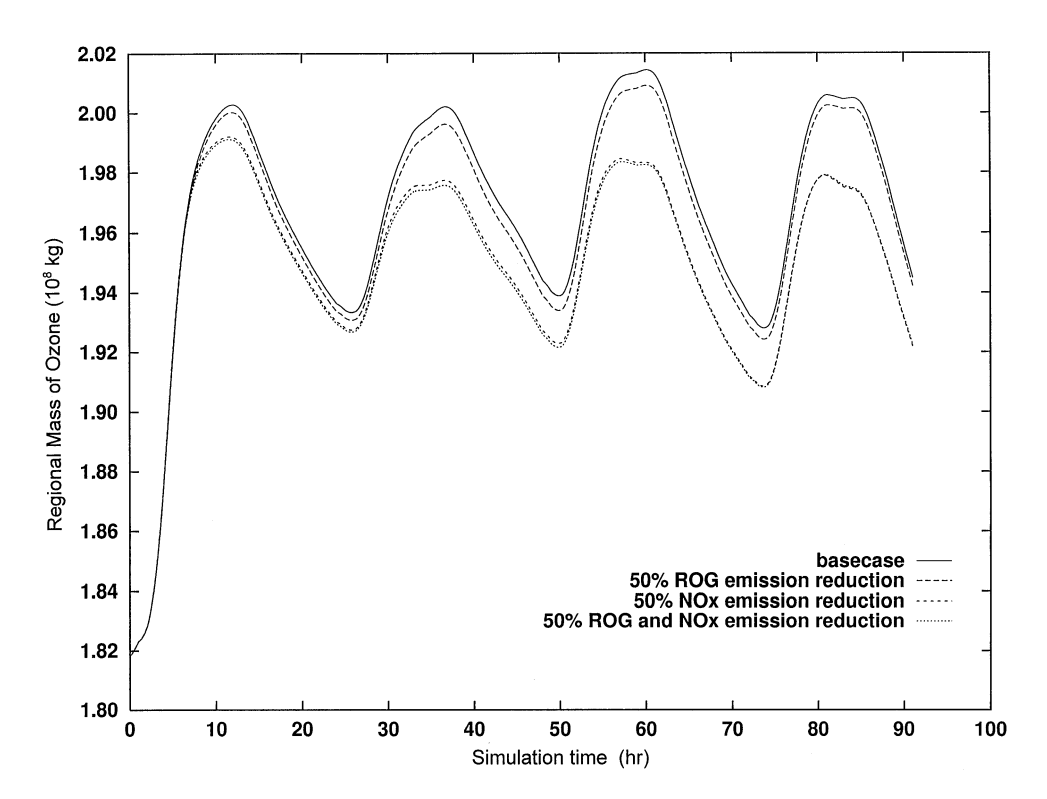


Fig. 9. Total ozone mass in the entire domain: base case predictions (solid), predictions with 50% ROG emission reduction (large dash), predictions with 50% NO_x emission reduction (small dash), and predictions with 50% NO_x and ROG emission reduction (dotted).

a significant impact on the San Joaquin Valley. During the study period the estimated mixing ratio of NO_x at the boundary was 3 ppb. Even though local emissions at certain locations can lead to levels exceeding 100 ppb, the

total mass of NO_x in the Valley that originates from the boundary is four times that emitted in the Valley itself. This is significantly different from many other areas, including the South Coast Air Basin of California, which

have weaker winds and higher emissions. A detailed description of the meteorology of the area for the same episode and its impact on air quality is presented by Niccum et al. (1995).

3.4. Effect of emissions

In order to study the effects of emissions in the Valley, a simulation was performed in which all of the ROG and NO_x emissions in the Valley were eliminated. With zero emissions, downwind concentrations should approach a level determined strictly by inflow conditions. In Arvin, with zero emissions there is a large reduction in daytime predicted ozone concentration (Fig. 6). The comparison of Fig. 6 with Fig. 4 (the case with zero boundary conditions) provides insight into the sources of ozone in Arvin. Fig. 6 shows that an ozone mixing ratio of approximately 50 ppb is the result of boundary conditions of about 40 ppb of ozone itself plus 10 ppb of ozone from ROG and NO_x precursors brought in across the boundary, while Fig. 4 shows the daytime peaks are a result of emissions. Recent estimates for the Eastern United States show ozone production efficiencies of about 3 per NO_x , so the 10 ppb of O_3 estimated to be attributable to boundary NO_x is consistent with these findings.

As seen earlier, emissions that affect Arvin are transported from upwind locations. In all locations of the Valley, emissions play a much larger role in the daytime peak concentrations of ozone than in the nighttime concentrations.

Fresno also exhibits a greatly decreased daytime ozone peak under zero emissions, partially a result of the lack of local emissions, and partially because of the removal of transported emissions. A point of interest in Fresno is an increase in nighttime ozone in the absence of emissions. This occurs in many populated areas of the Valley. In the populated areas when emissions are present, NO provides a significant sink for ozone at night. With the decreased level of NO in the zero emissions case, an increased level of nighttime ozone is predicted. Changes in Livermore ozone from zero emissions are smaller than at the other locations, with only slightly lower daytime peaks, and slightly higher nighttime lows.

3.5. ROG vs NO_x reduction

This section examines the impact of reducing ROG vs. NO_x emissions to determine whether areas of the Valley are ROG- or NO_x -controlled with respect to ozone formation. Ozone mixing ratios decrease at all sites at all

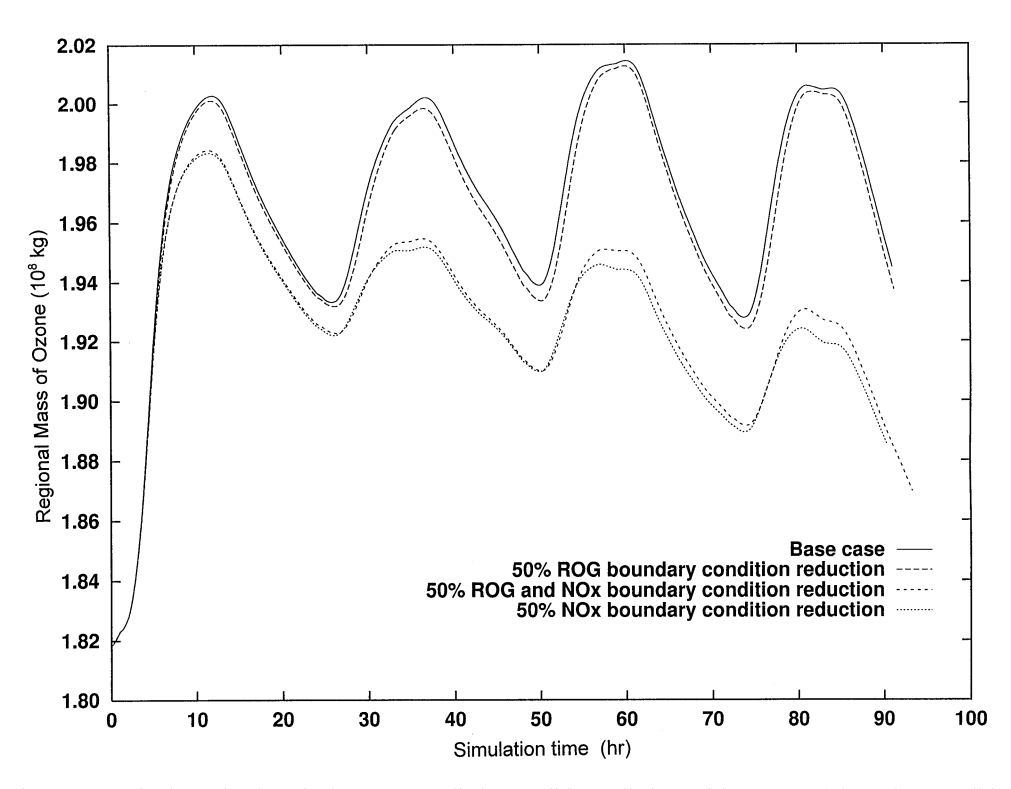


Fig. 10. Total ozone mass in the entire domain: base case predictions (solid), predictions with 50% ROG boundary condition reduction (large dash), predictions with 50% NO_x and 50% NO_x boundary condition reduction (small dash), and predictions with 50% NO_x boundary condition reduction (dotted).

times when ROG emissions are reduced by 50% (Fig. 7). A 50% reduction of NO_x , presented in Fig. 8, leads to two distinct regimes: a high NO_x regime where ozone mixing ratios increase and a low NO_x regime where ozone mixing ratios decrease. Ozone is predicted to be reduced more effectively by ROG control when NO_x concentrations exceed about 10 ppb. Similarly, NO_x control is predicted to be more effective when NO_x concentrations are lower than that threshold. A similar pattern of ozone dependence on ROG and NO_x reductions has been reported for the South Coast Air Basin by Milford et al. (1994).

The findings in Figs. 7 and 8 suggest the following questions: How would ROG and NO_x emission control affect ozone mixing ratios in the entire San Joaquin Valley? How does ROG and NO_x boundary condition reduction affect ozone mixing ratios in the entire Valley? Fig. 9 shows the integrated total ozone mass in the Valley for the base case and for three emission reduction scenarios: 50% ROG emission reduction only, 50% NO_x reduction only, and 50% reduction in the emissions of both ROG and NO_x . It is clearly seen that, on the whole, ozone is most sensitive to NO_x emissions. Fig. 10 shows ozone also being most sensitive to NO_x reduction at the

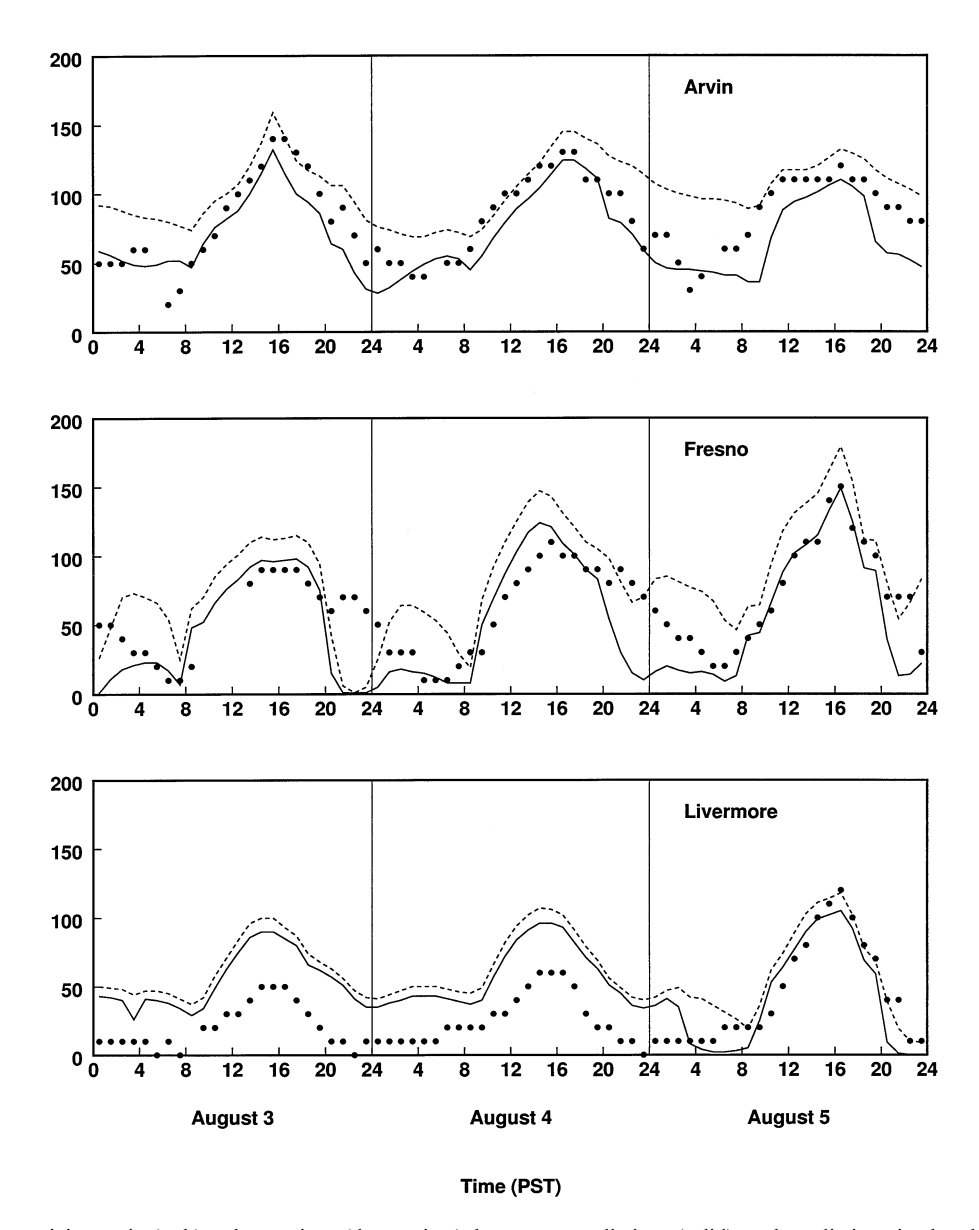


Fig. 11. Ozone mixing ratio (ppb): observations (data points), base case predictions (solid), and predictions in the absence of dry deposition (dashed).

boundary. Furthermore, a reduction in NO_x at the boundary has a greater impact on overall ozone mass in the Valley than NO_x emission reduction.

3.6. Dry deposition effect

A simulation in which dry deposition for all species is ignored allows one to determine the influence of dry deposition on predicted species levels. It is expected that sites that are farthest downwind will be most sensitive to perturbations of deposition velocities. Although there is a general increase in ozone concentration everywhere in the Valley when dry deposition is ignored, the sensitivity of Livermore ozone to zero dry deposition is significantly smaller than that at Arvin or Fresno, which are farther downwind (Fig. 11). Increase of ozone with zero dry deposition is also a result of slightly higher levels of NO_x, but this effect is significantly smaller than that of the direct removal of ozone itself.

The greatest sensitivity to dry deposition in Arvin and Fresno is at nighttime, which is true in most areas of the Valley. This demonstrates that dry deposition represents a nighttime ozone sink. The importance of dry deposition at night is likely a result of nighttime wind speeds, as wind speed and dry deposition rate are correlated.

As mentioned earlier, NO is also a major nighttime ozone sink for the more populated areas of the Valley. This explains the low nighttime ozone levels in Fresno, where both sinks are significant.

4. Conclusion

Several aspects of air quality in the San Joaquin Valley of central California have been revealed from systematic diagnostic runs of the SARMAP Air Quality Model. The air quality problem of the Valley is found to be fundamentally different from those in the South Coast Air Basin of California and other meteorologically isolated metropolitan areas. In such areas most species are locally emitted, whereas in the San Joaquin Valley a complex combination of local and transported emissions exists.

Significant inflow to the Valley imposes a strong dependence on boundary concentrations of pollutants. In the absence of any emissions in the modeling region, the boundary conditions produce a relatively constant ozone mixing ratio of approximately 50 ppb in most places in the Valley. Emissions are then primarily responsible for daytime peaks in ozone. The specific balances between boundary concentrations and emissions vary within the Valley according to location and population density. However, the integrated ozone mass of the entire region is more sensitive to boundary conditions than local emissions. In particular, our simulations show that for both sources of precursors, local emissions and boundaries,

 NO_x has a greater impact on ozone production than ROG.

Acknowledgements

We wish to thank Dr. Saffet Tanrikulu for making SAQM available to us and for his valuable assistance in the project. This work was supported by the California Air Resources Board, Exxon Education Foundation and the IBM Environmental Research Program. Any opinions, findings and conclusions or recommendations expressed in this material are those of the authors and do not necessarily reflect the views of the IBM Corporation or the Exxon Education Foundation. Fig. 2 was created using GrADS.

References

- Blumenthal, D.L., 1993. Field Study Plan for the San Joaquin Valley Air Quality Study (SJVAQS) and the Atmospheric Utility Signatures, Predictions, and Experiments (AUSPEX) Program. Final Report to California Air Resources Board, STI-98020-1241-FR. Sacramento, CA.
- Bott, A., 1989a. A positive definite advection scheme obtained by nonlinear renormalization of the advective fluxes. Monthly Weather Reviews 117, 1006–1015.
- Bott, A., 1989b. Reply. Monthly Weather Reviews 117, 2633–2636.
- Chang, J.S., Brost, R.A., Isaksen, I., Madronich, S., Middleton, P., Stockwell, W.R., Walceck, C.J., 1987. A three-dimensional Eulerian acid deposition model: physical concepts and formation. Journal of Geophysical Research 92, 14681–14700
- Chang, J.S., Jin, S., Li, Y., Beauharnois, M., Chang, K.-H., Huang, H.-C., Lu, C.-H., Wojcik, G., Tanrikulu, S., DaMassa, J., 1996. The SARMAP Air Quality Model. Part 1 of SAQM Final Report. California Air Resources Board, Sacramento, CA.
- Dabdub, D., Seinfeld, J.H., 1994. Numerical advective schemes used in air quality models—sequential and parallel implementation. Atmospheric Environment 28, 3369-3385.
- DaMassa, J., Tanrikulu, S., Magliano, K., Ranzieri, A.J., Niccum, E., 1996. Performance Evaluation of SAQM in Central California and Attainment Demonstration for the 3-6 August 1990 Ozone Episode. California Air Resources Board, Sacramento, CA.
- Gery, M.W., Whitten, G.Z., Killus, J.P., Dodge, M.C., 1989.
 A photochemical kinetics mechanism for urban and regional scale computer modeling. Journal of Geophysical Research 94, 12925–12956.
- Grell, G.A., Dudhia, J., Stauffer, D.R., 1993. A description of the fifth-generation penn state/NCAR mesoscale model (MM5). NCAR Tech. Note, NCAR/TN-398 + 1A.
- Hubbe, J.M., Pederson, J.R., 1994. Dry deposition study planning. In: Solomon, P.A., (Ed.), Planning and Managing Regional Air Quality. Lewis Publishers, Florida, in conjunction with Pacific Gas and Electric Company.

- Lagarias, J.S., Sylte, W.W., 1991. Designing and managing the San Joaquin Valley, air quality study. Journal of Air and Waste Management Association 41, 1176–1179.
- Magliano, K.L., 1994. Summary of SARMAP emissions modeling. Technical Support Division, California Air Resources Board, Sacramento, CA.
- McRae, G.J., Goodin, W.R., Seinfeld, J.H., 1982. Numerical solution of the atmospheric diffusion equation for chemically reacting flows. Journal of Computational Physics 45, 1–42.
- Milford, J.B., Gao, D., Sillman, S., Blossey, P., Russell, A.G., 1994. Total reactive nitrogen (NO_y) as an indicator of the sensitivity of ozone to reductions in hydrocarbon and NO_x emissions. Journal of Geophysical Research 99, 3533–3542.
- Niccum, E.M., Lehrman, D.E., Knuth, W.R., 1995. The influence of meteorology on the air quality in the San Luis Obispo County—Southwestern San Joaquin Valley region for 3–6 August 1990. Journal of Applied Meteorology 34, 1834–1847.
- Ranzieri, A.J., Thuillier, R.H., 1994. SJVAQS and AUSPEX: a Collaborative Air Quality Field Measurement and Modeling Program. Solomon, P.A. (Ed.), Planning and Managing Regional Air Quality, Lewis Publishers, Florida, in conjunction with Pacific Gas and Electric Company.

- Roberts, P.T., Lindsey, C.G., Smith, T.B., 1995. Analyses of San Joaquin Valley Air Quality and Meteorology. In: Solomon, P.A. (Ed.), Planning and Managing Regional Air Quality. Lewis Publishers, Florida, in conjunction with Pacific Gas and Electric Company.
- Seaman, N.L., Stauffer, D.R., Lario-Gibbs, A.M., 1995. A multi-scale four dimensional data assimilation applied in the San Joaquin valley during SARMAP. Part I: modeling design and basic performance characteristics. Journal of Applied Meteorology 34, 1739–1761.
- Smolarkiewicz, P.K., 1983. A simple positive-definite advection scheme with small implicit diffusion. Monthly Weather Reviews 111, 479–486.
- Smolarkiewicz, P.K., 1984. A fully multi-dimensional positivedefinite advection scheme with small implicit diffusion. Journal of Computational Physics 54, 325–362.
- Winner, D.A., Cass, G.R., Harley, R.H., 1995. The effect of alternative boundary conditions on predicting ozone control strategy performance: a case study in the Los Angeles area. Atmospheric Environment 29, 3451–3454.
- Yanenko, N.N., 1971. The Method of Fractional Steps. Springer, New York.